processes

MDPI

Article

Ionic Equilibria in Polytungstate Melts

Alexander V. Kosov *, Olga L. Semerikova, Sergey V. Vakarin, Olga V. Grishenkova, Alexey S. Vorob'ev, Anastasia O. Khudorozhkova and Yury P. Zaikov

Department of Electrolysis, Institute of High Temperature Electrochemistry, Ural Branch of the Russian Academy of Sciences, Yekaterinburg 620990, Russia
* Correspondence: alexander.kosoff@yandex.ru

Abstract: Polytungstate melts are used for the electrodeposition of oxide tungsten bronzes (OTBs). The scarce information on the ionic composition and properties of these electrolytes hinders effective control of the electrochemical synthesis of OTBs with desired electrical and optical properties. In this work, a comprehensive study of Na_2WO_4–WO_3 melts that contained up to 55 mol% of tungsten trioxide was performed in the temperature range from 983 to 1073 K. Melt densities were measured using the Archimedes method. DFT calculations were carried out for various tungsten-containing compounds, including $W_xO^{2+}_{3x-1}$, $W_xO^{2-}_{3x+1}$, $NaW_xO^{-}_{3x+1}$, and $Na_2W_xO_{3x+1}$. The calculated values of the W–O bond energy indicate that the tested compounds are stable in the specified temperature range, and the WO_2^{2+} cation is the most stable. The experimental dependences of the redox potential on the mole fraction of tungsten trioxide in the Na_2WO_4–WO_3 melt were obtained using the EMF method. A model that considers the processes of interaction between tungsten-containing ions and O^{2-} ions was proposed for the quantitative interpretation of these dependences. The equilibrium constants were found through fitting according to the Levenberg–Marquardt algorithm. The effect of the WO_3 mole fraction and temperature on the concentrations of WO_4^{2-}, $W_2O_7^{2-}$, $W_3O_{10}^{2-}$, $W_4O_{13}^{2-}$, WO_2^{2+}, and O^{2-} ions was analyzed.

Keywords: EMF method; platinum reference electrode; ionic composition model; melting process; polytungstate melt density; DFT calculation

check for updates

Citation: Kosov, A.V.; Semerikova, O.L.; Vakarin, S.V.; Grishenkova, O.V.; Vorob'ev, A.S.; Khudorozhkova, A.O.; Zaikov, Y.P. Ionic Equilibria in Polytungstate Melts. *Processes* **2022**, *10*, 2658. https://doi.org/10.3390/pr10122658

Academic Editor: Haiyan Wang

Received: 10 November 2022
Accepted: 6 December 2022
Published: 9 December 2022

1. Introduction

Oxide tungsten bronzes (OTBs), i.e., nonstoichiometric compounds such as M_xWO_3 (here, M is an alkali metal and $0 < x < 1$), have a wide range of composition-dependent properties [1,2]. The diverse electrophysical and optical properties of M_xWO_3 with different x and M [1–6] determine the broad use of OTBs in many fields of catalysis [7–9] and photocatalysis [10–12], including air and wastewater purification, anti-virus sterilization and hydrogen and oxygen production. OTB-based materials are also in demand for electrochromic [13], plasmonic [14], innovative biomedical [15] and field emission [16] applications, and NIR shielding [17].

Electrodeposition from polytungstate melts is one of the most promising methods for the synthesis of OTBs [18–21] and multilayered hybrid systems with nanocrystalline OTBs [9,22–24]. The main advantages of this method are the high process rate, the ability to change the composition and structure of deposits by varying the electrolysis parameters, and low capital and operating costs. Evidently, understanding the regularities of the processes that occur in the polytungstate electrolyte and at the electrolyte/electrode interface is necessary for efficient control of electrodeposition and obtaining OTBs with the desired physicochemical properties. However, the mechanism of OTB electrocrystallization is difficult to determine without the availability of sufficient information on the structure and ionic composition of polytungstate melts. The limited data lead to the emergence of unfounded hypotheses about the mechanisms of OTB formation in these melts [21,25–28].

The structures of molten Na_2WO_4 at 1033 K [29] and $Na_2W_2O_7$ at 1087 K [30] were investigated using the radial distribution function based on X-ray scattered intensity data. The presence of tetrahedral $(WO_4)^{2-}$ anions in molten Na_2WO_4 was proven [29]. In the Na_2WO_4–WO_3 (1:1) system [30], it was found that the pattern of the $[(W_2O_7)^{2-}]_\infty$ anion chain in the crystalline state is practically preserved in the molten state within a small range (<0.45 nm), but the long-range order within one anion chain is almost lost in the melt and the neighboring chains are randomly oriented relative to each other. A Raman scattering study of molten alkali–metal tungstates [31,32] and transparent glasses obtained by rapid quenching of ditungstate melts [32] showed the presence of isolated $[WO_4]^{2-}$ tetrahedral anions in Na_2WO_4 and K_2WO_4 melts and complexes that consisted of two corner-sharing tetrahedra (i.e., $[W_2O_7]^{2-}$) in $Na_2W_2O_7$ and $K_2W_2O_7$ melts. The vibration modes of $[W_2O_7]^{2-}$ dimers were also found during the study of the microstructure of molten $M_2W_2O_7$ (M = Li, Na, K) by in situ high-temperature Raman spectroscopy, in combination with density functional theory (DFT) analysis [33,34]. The cation influence is mainly limited by the change in the characteristics of the W–O_{nb} bond (nb is non-bridging oxygen) in $[W_2O_7]^{2-}$ [31,33]. A joint analysis of the data of in situ high-temperature Raman spectroscopy and a quantum-chemical ab initio calculation for the evolution of stably existing structural units in Li_2O–WO_3 melts was carried out in [35]. It was concluded that complexes ($[WO_4]^{2-}$) and chains ($[W_2O_7]^{2-}$, $[W_3O_{10}]^{2-}$, and $[W_4O_{13}]^{2-}$) composed of two, three, or four $[WO_4]^{2-}$ are formed by sharing their corner oxygen atoms when the mole ratio of Li_2O:WO_3 in the melt is 1:1, 1:2, 1:3, and 1:4, respectively [35]. Raman spectroscopy or X-ray scattering data for the M_2O–WO_3 melts with any intermediate component ratio (for example, 1:1.5) are not available, which does not allow us to predict changes in the structure or structure-dependent properties of M_2WO_4–WO_3 melts.

The data obtained by the EMF method can be used to estimate the ratio of anions in polytungstate melts [18,36–38]. The approach is based on the analysis of the experimental dependence of the potential difference between two platinum–oxygen electrodes semi-immersed in melts with different concentrations of tungsten trioxide (the melts are separated by a porous diaphragm); assumptions about ionic equilibria are required for analysis. In [18], this method was applied to determine the $WO_4^{2-}/W_2O_7^{2-}$ ratios in Na_2WO_4–M'_2WO_4–WO_3 (M^* = Li or K) melts that contained up to 20 mol% WO_3. The results of [18] satisfactorily explained the change in the OTB composition with an increase in the tungsten trioxide content in the above concentration range. The M_2WO_4–WO_3 melts with a WO_3 mole fraction up to 0.5 were studied using the EMF method in [38]. The authors considered these melts as completely dissociated mutual solutions of Na_2WO_4 and $Na_2W_2O_7$ that consisted of an ion mixture (Na^+, WO_4^{2-}, and $W_2O_7^{2-}$). A conclusion was made about the weak interionic interaction in this system. An acceptable agreement was achieved between the experimental and calculated results at a WO_3 mole fraction up to 0.4 by introducing the activity coefficients of ditungstate ions [38]. According to [18,38], a model that considers the formation of $W_3O_{10}^{2-}$ and $W_4O_{13}^{2-}$ is required to more accurately describe the experimental results at high WO_3 concentrations in melts.

The above literature data confirm that polytungstate melts contain various tungsten-containing anions and alkali metal cations. However, it is unlikely that the anions are directly involved in the cathodic process that leads to the electrodeposition of OTB and/or tungsten on the cathode. An assumption was made in [18] about the formation of W^{6+} cations as a result of the following processes:

$$4W_2O_7^{2-} \rightleftarrows 7W_2O_7^{2-} + W^{6+}, \quad (1)$$

$$7W_4O_{13}^{2-} \rightleftarrows 13W_2O_7^{2-} + 2W^{6+} \quad (2)$$

However, the authors provide no evidence to support this hypothesis. Thus, the problem of the ionic composition and its changes as the proportion of tungsten trioxide in the melt increases remains topical.

In this work, the stability of various tungsten-containing anions and cations is evaluated, and a model is proposed for calculating the ionic composition of Na_2WO_4–WO_3 melts with a WO_3 mole fraction up to 0.55.

2. Materials and Methods

2.1. Preparation of Electrolytes

Sodium tungstate and tungsten trioxide (purity 99.9 wt%, Vecton, RF) were used to prepare the melts. The dried (523 K, 2 h) reagents were weighed using a VK-600 balance (Massa-K, RF) with an accuracy of ±0.01 g, and then the electrolyte components were mixed in the required proportions in a porcelain container. The WO_3 mole fraction in the mixtures, ν, ranged from 0 to 0.55. The prepared mixtures were placed in platinum or alumina crucibles (see Sections 2.2 and 2.3) and heated to the experimental temperature (983, 1023 or 1073 K). In accordance with the phase diagram of the Na_2WO_4–WO_3 system [18], the composition range was limited to $0 \leq \nu \leq 0.40$ at 983 K and $0 \leq \nu \leq 0.55$ at 1023 and 1073 K, respectively.

2.2. Electrochemical Measurements

All the electrochemical measurements were performed using Autolab PGSTAT302N (Metrohm, The Netherlands) with Nova 1.9 software. Figure 1 shows the electrochemical cell designs described in detail in Sections 2.2.1 and 2.2.2.

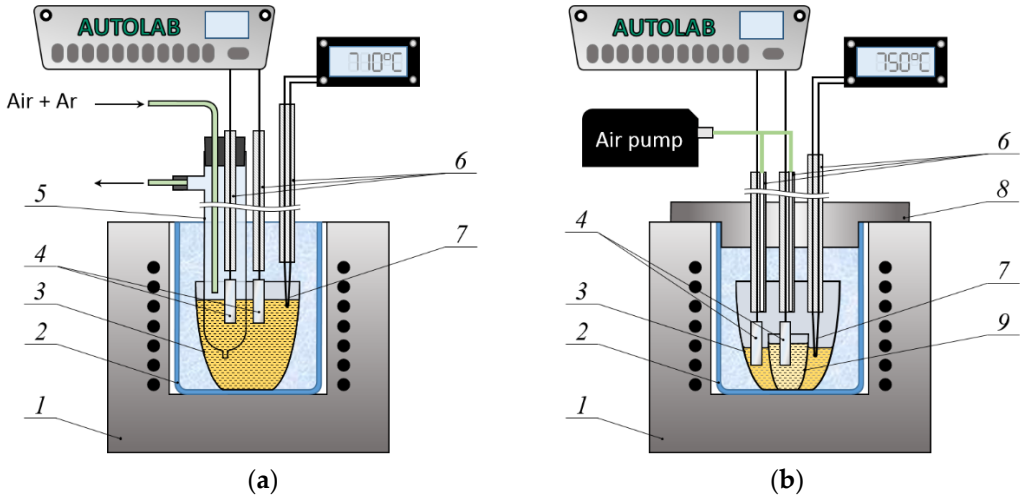

Figure 1. Schemes of experimental setups (**a**) for determining the effect of oxygen partial pressure on the potential of the Pt electrode and (**b**) for measuring the dependence of ΔE on the mole fraction of WO3 in the melt. Designations: *1*—shaft furnace, *2*—quartz protective vessel, *3*—platinum crucible with the 0.8Na2WO4–0.2WO3 melt (standard melt), *4*—Pt electrodes, *5*—quartz test tube, *6*—alumina tubes, *7*—Pt/Pt-Rh thermocouple, *8*—stainless steel lid filled with kaolin wool, *9*—thin-walled alumina crucible with the melt under study.

All high-temperature experiments were carried out in a shaft furnace with a quartz protective vessel installed inside. The melt temperature was controlled using a Pt/Pt-Rh thermocouple and a Varta TP703 temperature controller (Varta, RF) with an accuracy of ±1 K. The operating temperature range corresponded to the usual conditions for OTB electrodeposition from Na_2WO_4–WO_3 melts.

2.2.1. Measurement of the Oxygen Function of the Pt Electrode

The dependences of the potential difference between two Pt electrodes half-immersed in the melt on the partial pressure of oxygen over one of the electrodes were measured at 983 K. This was carried out to confirm that the reaction

$$\frac{1}{2}O_2 + 2e \rightleftarrows O^{2-} \quad (3)$$

is the potential-determining process of the platinum–oxygen electrode. Both electrodes were made of Pt foil; the surface area of each electrode was S = 0.9 cm^2. Before measurements, one of the electrodes and a quartz test tube equipped with a vacuum rubber stopper, a spout for gas removal, and a bottom channel for electrolyte inflow were lowered into the $0.8Na_2WO_4$–$0.2WO_3$ melt in a platinum crucible (Figure 1a). The Pt electrode and a quartz tube for supplying a mixture of air with high-purity argon (99.999%, Uralcryogas, RF) were inserted into the stopper holes beforehand. The volume fraction of air in the gas flow was changed using a mass flow controller (LOW-ΔP-FLOW F-201DV) and a mass flow meter (LOW-ΔP-FLOW F-101D) for low pressure drops or corrosive gas (Bronkhorst High-Tech B.V., Ruurlo village, The Netherlands).

2.2.2. EMF Measurement

The EMF of the cell

$$\mathrm{Pt,\ O_2(air)|0.8Na_2WO_4{-}0.2WO_3\,\vdots\,(1-\nu)Na_2WO_4{-}\nu WO_3\,|O_2(air),\ Pt} \quad (4)$$

was measured at 983, 1023 and 1073 K in air (p_{O_2}= 21.3 kPa). The cell design is presented in Figure 1b. A small thin-walled alumina crucible 1.8 cm in diameter with the $(1-\nu)Na_2WO_4$–νWO_3 melt was placed on the bottom of a platinum crucible 3.5 cm in diameter, which served as a container for the standard melt ($0.8Na_2WO_4$–$0.2WO_3$ in this work). The electrodes (Pt foil, S = 0.9 cm^2) were half-immersed in the above melts before measurements. Alumina tubes protected the platinum current leads; air was blown through the second opening of these tubes. The recording of the potential difference was stopped when the ΔE value remained constant (within ±0.5 mV) for 30 min.

2.3. Density Measurement

The densities of the Na_2WO_4–WO_3 melts with a mole fraction of tungsten trioxide up to 0.5 were measured using the Archimedean method, according to the technique described in [39,40]. A platinum sphere was suspended on a platinum wire 0.5 mm in diameter and 0.6 m long attached to a Mettler AT20 analytical balance (Mettler Toledo, Billerica, MA, USA). A weighed amount of a prepared oxide–salt mixture was placed in an alumina crucible. The measurements were performed within a temperature range from 983 K to 1073 K. The platinum sphere was placed into the melt at 1073 K, and temperature dependence of the sphere weight was registered. The density was calculated according to the equation

$$\rho = \Delta m / V_s, \quad (5)$$

where Δm (g) is the difference between the sphere weight in the melt and in air, and V_s (cm^3) is the sphere volume. The cargo weight in the air was 14.5126 g. The temperature dependence of the sphere volume was determined by calibration using molten chlorides [40]. The experimental error for the density did not exceed ±0.5%.

2.4. Density Functional Theory (DFT) Calculations

Calculations of the stability of tungsten-containing compounds ($W_xO^{2+}_{3x-1}$, $W_xO^{2-}_{3x+1}$, $NaW_xO^{-}_{3x+1}$, and $Na_2W_xO_{3x+1}$) were performed using the Siesta software package [41] on a cluster-type hybrid computer with 1864 CPUs and a peak performance of 216 Tflops. Geometric optimization was carried out using the general gradient approximation method in the PBE form [42] for all proposed systems. The dynamic relaxation of atoms continued until the change in the total energy of the system became less than 0.1 meV. The cutoff energy of the plane wave basis was 400 Ry. A cubic unit cell with a face translation vector of 20 Å was used. After geometric optimization, the resulting systems were tested for temperature stability using ab initio molecular dynamics with a Nose–Hoover thermostat [43] at 983, 1023 and 1073 K for 1000 time steps with a step of 1 fs.

3. Experimental Results

3.1. Electrochemical Measurements

The data obtained in the experiment described in Section 2.2.1 and their analysis are shown in Figure 2. Figure 2a demonstrates the experimental dependence of the potential difference, ΔE (V), between two Pt electrodes half-immersed in the $0.8Na_2WO_4$–$0.2WO_3$ melt with a stepwise change in the volume fraction of air in the gas mixture, W_{air} (vol%), above one of the electrodes. Evidently, an increase in W_{air} causes a decrease in the ΔE value. The dependence of ΔE on the logarithm of the air volume fraction is linear (Figure 2b) and the slope is close to theoretical one, as shown in the following equation:

$$\Delta E = \frac{kT}{4e} \ln \frac{[O_2]_1}{[O_2]_2} = \frac{kT}{4e} \ln \frac{p_{O_2\ air} W_{air}}{p_{O_2\ air}} = 21.54 \cdot 10^{-3} T \ln W_{air}, \quad (6)$$

where k (1.38×10^{-23} J K^{-1}) is the Boltzmann constant, T (K) is the absolute temperature, e (C) is the elementary electric charge, $[O_2]_1$ and $[O_2]_2$ (mol L^{-1}) are the concentrations of oxygen in the atmosphere above the first and second Pt electrodes, respectively (see Figure 1a), and $p_{O_2\ air}$ is the partial pressure of oxygen in air. The error is small and equal to 0.39%. Formula (6) was derived using the Nernst equation for Reaction (3) and is as follows:

$$E = E^0 + \frac{kT}{2e} \ln \frac{[O_2]^{\frac{1}{2}}}{[O^{2-}]}, \quad (7)$$

where E^0 (V) is the standard electrode potential and $[O_2]$ and $[O^{2-}]$ (mol L^{-1}) are the concentrations of oxygen (above the melt) and O^{2-} ions (in this melt), respectively. This means that the potential of the platinum electrode is indeed determined by Reaction (3).

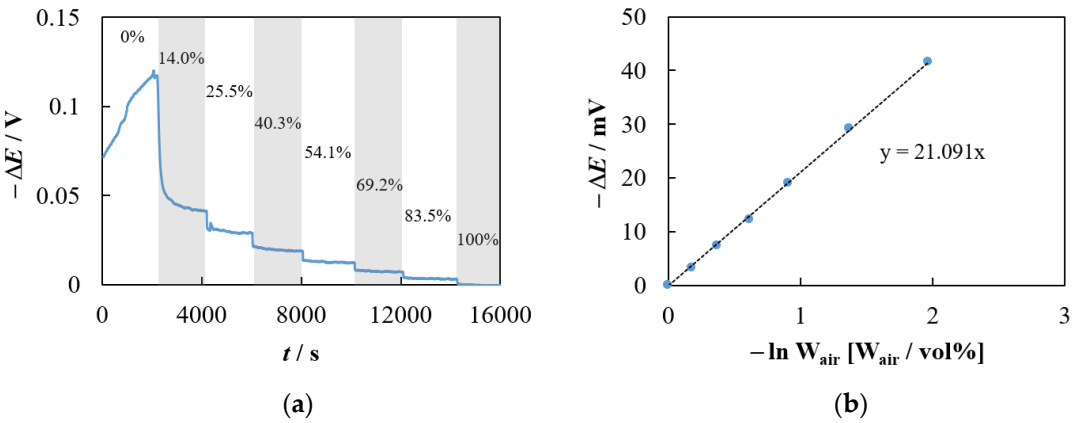

Figure 2. (**a**) Experimental time dependence of the potential difference between two platinum–oxygen electrodes with a stepwise change in the volume fraction of air, W_{air}, above one of them. The W_{air} (vol%) values are shown in the figure. T = 983 K. Other details of the experiment are described in Section 2.2.1. (**b**) Dependence of the potential difference on the logarithm of the volume fraction of air.

In this case, the potential difference measured in Cell (4) is described by the following equation:

$$\Delta E = \frac{kT}{2e} \ln \frac{[O^{2-}]_{melt\ 1}}{[O^{2-}]_{melt\ 2}}, \quad (8)$$

This allows us to find the ratio of oxide–ion concentrations in melts with different WO_3 contents. Equation (8) can be rewritten as follows:

$$\Delta E = \frac{kT}{2e} \ln \frac{g_1 V_{m2}}{g_2 V_{m1}}, \quad (9)$$

where g (mol) is the amount of O^{2-} ions in the melt, V_m (cm^3 mol^{-1}) is the molar volume of the melt, and subscripts 1 and 2 refer to the $(1 - \nu)Na_2WO_4$–νWO_3 melt and the standard melt ($0.8Na_2WO_4$–$0.2WO_3$ in this work), respectively.

The experimental concentration dependences of ΔE measured in Cell (4) at 983, 1023 and 1073 K are shown in Figure 3. Since the decrease in ΔE is associated with a change in the O^{2-} concentration in the melt due to an increase in the WO_3 mole fraction (see Equation (8)), these experimental dependences can be interpreted as follows. In pure molten sodium tungstate, the O^{2-} concentration is significantly higher than in the standard melt (by six orders of magnitude at 983 K). A sharp decrease in the O^{2-} concentration occurs when the WO_3 mole fraction is only 0.01 (about 4 orders of magnitude at 983 K). In the range of ν from 0.05 to 0.55, the concentration of O^{2-} ions decreases approximately according to the logarithmic law, since the $\Delta E(\nu)$ dependences decrease almost linearly. At 1073 K, the range of the O^{2-} concentration becomes noticeably narrower, as demonstrated by the ΔE values at $\nu = 0$ and $\nu > 0.4$ (see Figure 3).

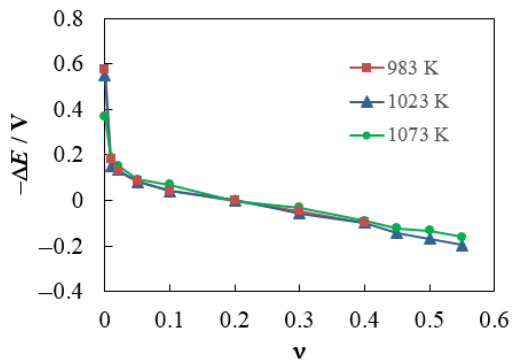

Figure 3. Experimental dependences of the potential difference in Cell (4) on the WO_3 mole fraction in the $(1 - \nu)Na_2WO_4$–νWO_3 melt at 983, 1023 and 1073 K.

The quantitative interpretation of these data is difficult because the dependences of g and V on the WO_3 mole fraction are unknown. Dependences $V(\nu)$ can be found from the measured densities of melts with different contents of tungsten trioxide (see Section 3.2). The situation for $g(\nu)$ is much more complicated, since information is required on the processes in the melt and equilibria with the participation of O^{2-} ions, as well as on the corresponding equilibrium constants. The absolute values of the equilibrium concentrations of ions in the melt can be found only in this case.

The problem is that there is still no unambiguous opinion regarding the ionic composition of polytungstate melts. Published data [29–34] show that various polytungstate anions with the general formula $W_xO^{2+}_{3x-1}$ can exist in the melt. At the same time, the results obtained by electrochemical methods (see, for example, [9,18,21]) indicate the presence of tungsten-containing cations in the melt, but do not allow one to determine their composition and charge. Nevertheless, the hypothesis of the presence of W^{6+} ions in the melt seems unlikely, due to the high molecularity of Equilibria (1) and (2) and the high concentration of oxygen-containing ions. It is more likely that $W_xO^{2+}_{3x-1}$ cations can be formed as a result of the dissociation of $W_xO^{2-}_{3x+1}$ anions. However, we must ensure that $W_xO^{2+}_{3x-1}$ cations are stable at the experimental temperatures (see Section 4) before modeling equilibria that involve these cations (see Section 5).

3.2. Density Measurement

The experimental dependences of the density on the WO_3 mole fraction in $(1 - \nu)Na_2WO_4$–νWO_3 melts are shown in Figure 4. Figure 4a demonstrates that the decrease in density occurs both with an increase in temperature and with a decrease in

ν. The measured dependences of density on temperature and concentration of tungsten trioxide can be described by the following equations:

$$\rho = -2.64 \cdot 10^{-3} \cdot T\nu - 7.69 \cdot 10^{-4} \cdot T + 3.781\nu + 4.555,\ 0 < \nu \leq 0.3, \quad (10)$$

$$\rho = -1.20 \cdot 10^{-3} \cdot T\nu - 1.01 \cdot 10^{-3} \cdot T + 2.362\nu + 4.816,\ 0.3 < \nu \leq 0.5. \quad (11)$$

Note that these dependences are much more accurate than the approximate equation proposed in [44] (see Figure 4a):

$$\rho = 4.808 + 1.282\,\nu - 0.962 \cdot 10^{-3} \cdot T,\ 0 \leq \nu \leq 0.2. \quad (12)$$

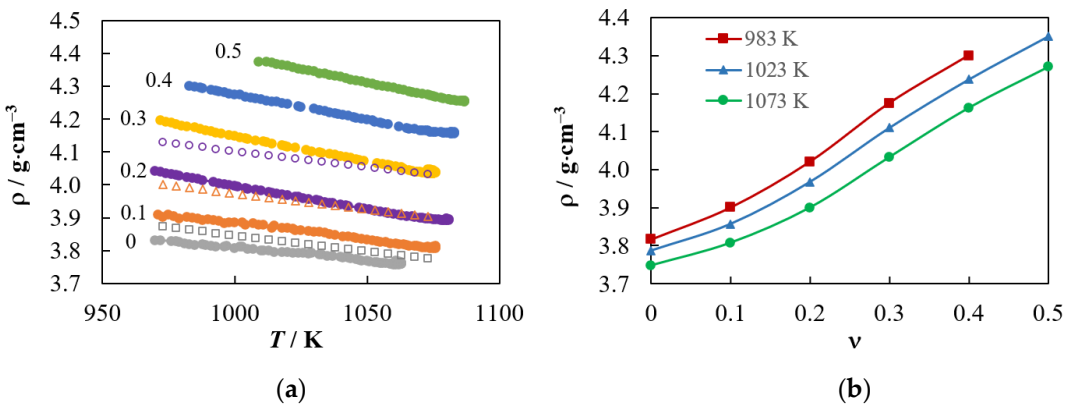

Figure 4. (**a**) Experimental temperature dependences of the density of the $(1 - \nu)Na_2WO_4$–νWO_3 melts. The WO_3 mole fraction values (ν) are shown in the figure. Our results are compared with the calculation by Equation (12) [44] at a ν equal to 0 (□), 0.1(△) and 0.2(○). (**b**) Dependences of density on the WO_3 mole fraction at 983, 1023 and 1073 K.

The dependences of the density of the tested melt on the WO_3 mole fraction are presented in Figure 4b. These dependencies can be described by the equations

$$\rho(\nu) = -5.4406\nu^3 + 4.0947\nu^2 + 0.4392\nu + 3.8182,\ T = 983\ \text{K}, \quad (13)$$

$$\rho(\nu) = -3.8131\nu^3 + 3.3646\nu^2 + 0.3974\nu + 3.7866,\ T = 1023\ \text{K}, \quad (14)$$

$$\rho(\nu) = -3.7622\nu^3 + 3.513\nu^2 + 0.2277\nu + 3.7489,\ T = 1073\ \text{K}. \quad (15)$$

These equations are suitable for calculating the dependence of the molar volume of the melt on the WO_3 mole fraction.

$$V_m(\nu) = \left[(1-\nu)M_{Na_2WO_4} + \nu M_{WO_3}\right]/\rho(\nu), \quad (16)$$

where M (g mol^{-1}) is the molar mass.

4. DFT Calculation

To determine the stability of $W_xO^{2+}_{3x-1}$ and $W_xO^{2-}_{3x+1}$ compounds, the W–O bond energy, E_b (eV), was calculated according to the following formula:

$$E_b = -\left(E_{tot} - E_{1W}N_W - E_{1O}N_O\right)/N_b, \quad (17)$$

where E_{tot} (eV) is the total energy of the compound, E_{1W} and E_{1O} (eV) are the energies calculated for single W^{6+} and O^{2-} ions, respectively, N_W and N_O are the amount of tungsten and oxygen ions in the system, respectively, and N_b is the amount W–O bonds in the compound.

The W–O binding energies in the $NaW_xO^-_{3x+1}$ and $Na_2W_xO_{3x+1}$ compounds were calculated, taking into account the interaction of Na^+ with tungsten-containing anions.

$$E_b = (E_{tot} - E_b{}^{Na} - E_{1W}N_W - E_{1O}N_O)/N_b, \quad (18)$$

$$E_b{}^{Na} = E_{tot} - E_{WO} - E_{Na}, \quad (19)$$

where $E_b{}^{Na}$ (eV) is the binding energy between Na^+ and $W_xO^{2-}_{3x+1}$, E_{WO} (eV) is the energy calculated for the system without Na^+, and E_{Na} (eV) is the energy calculated for the sodium subsystem only.

The calculation results indicate that all the tested compounds are stable in the temperature range from 983 to 1073 K. The geometric structures of $W_xO^{2+}_{3x-1}$ and $W_xO^{2-}_{3x+1}$ at 983 K are shown in Figure 5a. An increase in temperature does not affect the geometric structure of the compounds in most cases. The only exception is the rearrangement of the $[W_4O_{13}]^{2-}$ compound at 1073 K (Figure 5b).

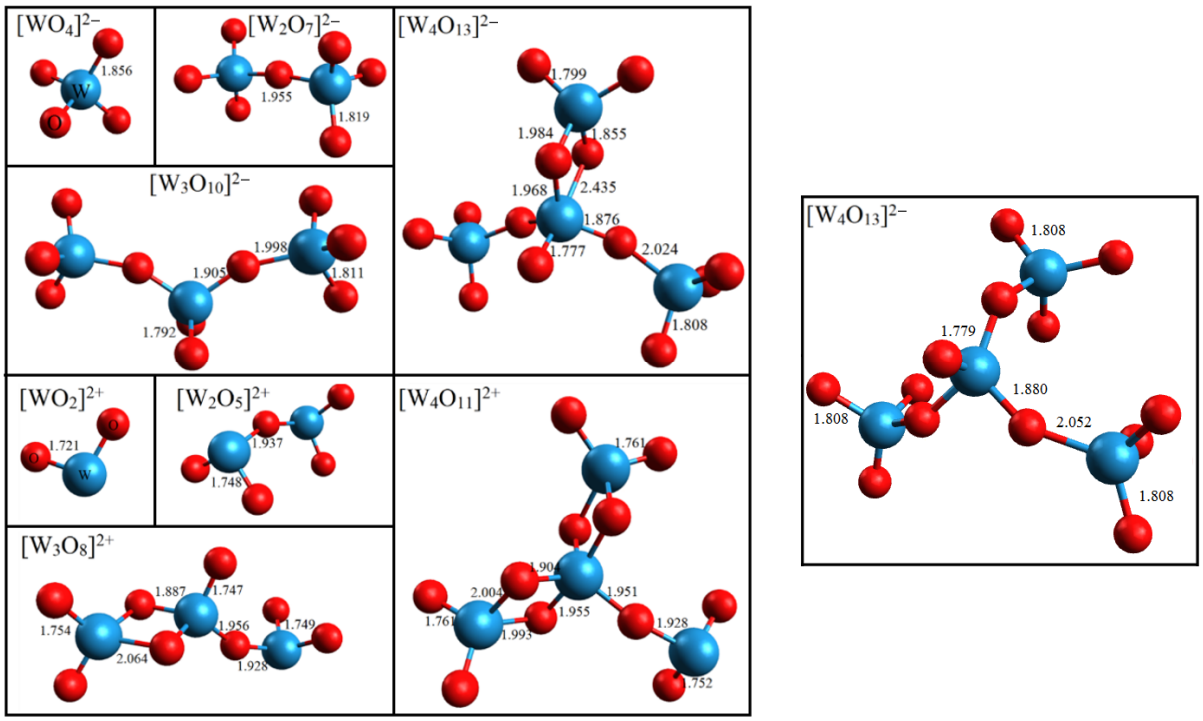

(**a**) (**b**)

Figure 5. (**a**) Geometric structures of $W_xO^{2-}_{3x+1}$ and $W_xO^{2+}_{3x-1}$ compounds after geometric optimization and ab initio molecular dynamics with a Nose–Hoover thermostat at 983 K. (**b**) Geometric structure of $[W_4O_{13}]^{2-}$ at 1073 K. Bond lengths are given in angstroms.

Figure 6a shows the dependences of the W–O bond energy on the number of tungsten atoms in $W_xO^{2+}_{3x-1}$, $W_xO^{2-}_{3x+1}$, $NaW_xO^-_{3x+1}$ and $Na_2W_xO_{3x+1}$ compounds at 983 K. The E_b value in $W_xO^{2+}_{3x-1}$ is lower than in $W_xO^{2-}_{3x+1}$ by 54% at x = 1 and by 6.7% at x = 4. The W–O bond energy for the WO^{2+}_2 cation is minimal (E_b = −105.48 eV), which indicates its high stability. An increase in the number of tungsten atoms in $W_xO^{2+}_{3x-1}$ and $W_xO^{2-}_{3x+1}$ leads to an increase in the E_b value from −105.48 to −66.13 eV and from −68.41 to −62.01 eV, respectively. The addition of one or two sodium ions to the second coordination sphere contributes to a decrease in the W–O bond energy; namely, the E_b values are 2.5–8.3% (for $NaW_xO^-_{3x+1}$) or 4.6–13.8% (for $Na_2W_xO_{3x+1}$) lower than those for $W_xO^{2-}_{3x+1}$.

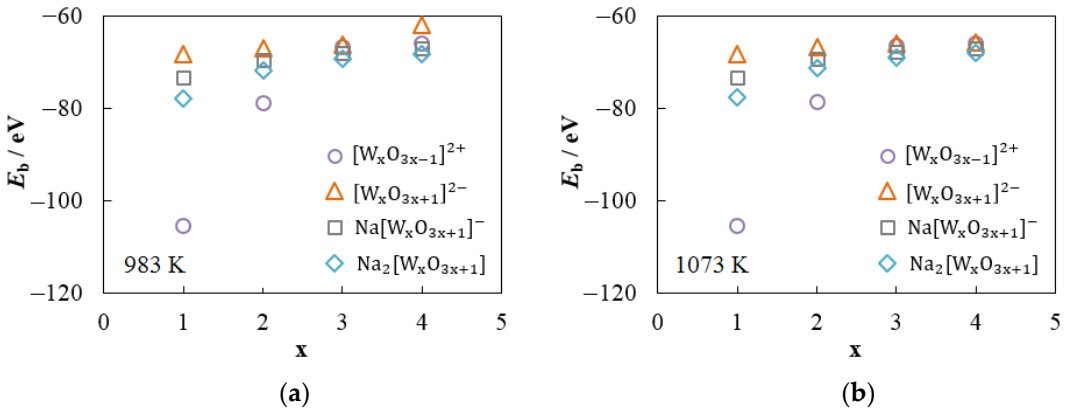

Figure 6. Dependences of W–O bond energy on the number of W atoms in the compound at (**a**) 983 K and (**b**) 1073 K.

At 1073 K, the E_b value increases slightly in most cases (Figure 6b). The maximum increase is observed for $Na_2[W_2O_7]$ and does not exceed 0.7%. On the contrary, the W–O bond energy in the $[W_4O_{13}]^{2-}$ compound decreases from −62.01 eV at 983 K to −65.71 eV at 1073 K, which is associated with the breaking of one W–O bond (see Figure 5).

5. Model of Ionic Equilibria

The above results of DFT calculations and published data [29–34] indicate the presence of several species of ions in the Na_2WO_4–WO_3 melt. The most probable set of ions includes Na^+, WO_4^{2-}, $W_2O_7^{2-}$, $W_3O_{10}^{2-}$, $W_4O_{13}^{2-}$, WO_2^{2+}, and O^{2-}. One can assume that the ratios between tungsten-containing ions depend on the WO_3 mole fraction in the initial oxide–salt mixture before its melting. If the initial mixture consists of ν mol of WO_3 and (1 − ν) mol of Na_2WO_4, then the melting process can be described as follows:

$$(1-\nu)Na_2WO_4 + \nu WO_3 = 2(1-\nu)Na^+ + aWO_2^{2+} + bWO_4^{2-} + cW_2O_7^{2-} + dW_3O_{10}^{2-} + fW_4O_{13}^{2-} + gO^{2-}, \quad (20)$$

where $0 \le \nu \le 0.55$ and the coefficients a, b, c, d, f, and g are equal to the number of moles of the corresponding ion if the total amount of the initial mixture is one mol. The balances of tungsten atoms and electric charges for reaction (20) give the following equalities::

$$a + b + 2c + 3d + 4f = 1, \quad (21)$$

$$b + c + d + f + g - a = 1 - \nu. \quad (22)$$

The tungsten-containing ions interact and are in dynamic equilibrium with each other and with O^{2-} ions.

$$WO_4^{2-} \rightleftarrows WO_2^{2+} + 2O^{2-},\ k_0 = \frac{\left[WO_2^{2+}\right]\left[O^{2-}\right]^2}{\left[WO_4^{2-}\right]} = \frac{ag^2}{bV_m^2}, \quad (23)$$

$$WO_4^{2-} + W_3O_{10}^{2-} \rightleftarrows 2W_2O_7^{2-},\ k_1 = \frac{c^2}{bd}, \quad (24)$$

$$W_2O_7^{2-} + W_4O_{13}^{2-} \rightleftarrows 2W_3O_{10}^{2-},\ k_2 = \frac{d^2}{cf}, \quad (25)$$

$$2WO_4^{2-} \rightleftarrows W_2O_7^{2-} + O^{2-},\ k_3 = \frac{cg}{b^2}, \quad (26)$$

$$3W_2O_7^{2-} \rightleftarrows 2W_3O_{10}^{2-} + O^{2-},\ k_4 = \frac{d^2g}{c^3}, \quad (27)$$

$$4W_3O_{10}^{2-} \rightleftarrows 3W_4O_{13}^{2-} + O^{2-},\ k_5 = \frac{f^3g}{d^4} \quad (28)$$

where k_0, k_1, k_2, k_3, k_4, and k_5 are the equilibrium constants of the corresponding processes. Equilibria (24) and (25) were written under the assumption that all the tungsten trioxide is consumed for the formation of tungsten-containing anions as a result of the reactions $WO_4^{2-} + WO_3 \rightarrow W_2O_7^{2-}$, $W_2O_7^{2-} + WO_3 \rightarrow W_3O_{10}^{2-}$, and $W_3O_{10}^{2-} + WO_3 \rightarrow W_4O_{13}^{2-}$.

It is easy to prove that the equilibrium constants k_3, k_4 and k_5 are interdependent, as demonstrated by the following equations:

$$g = k_3 \frac{b^2}{c} = k_4 k_1^2 \frac{b^2}{c} = k_5 k_1^2 k_2^3 \frac{b^2}{c}, \tag{29}$$

$$k_4 = \frac{k_3}{k_1^2},\ k_5 = \frac{k_3}{k_1^2 k_2^3}. \tag{30}$$

Therefore, only the constants k_0, k_1, k_2 and k_3 are required to determine the coefficients in Equation (20) for any ν value. Accordingly, the problem is reduced to solving a system of non-linear equations.

$$\begin{cases} a + b + 2c + 3d + 4f = 1 \\ b + c + d + f + g - a = 1 - \nu \\ \log a + 2\log g - \log b = \log k_0 + 2\log V_m \\ 2\log c - \log b - \log d = \log k_1 \\ 2\log d - \log c - \log f = \log k_2 \\ \log c + \log g - 2\log b = \log k_3 \end{cases}. \tag{31}$$

The values of the equilibrium constants that provide the best agreement between the experimental and calculated $\Delta E(\nu)$ dependences can now be found using a non-linear fit. As a result, $a(\nu)$, $b(\nu)$ $c(\nu)$, $d(\nu)$, $f(\nu)$, and $g(\nu)$ that correspond to the experimental conditions can be determined.

6. Results and Discussion

To calculate $\Delta E(\nu)$, Equation (32) was used in the following form:

$$\Delta E(\nu) = \frac{kT}{2e} \ln \frac{g(\nu) V_{m(\nu=0.2)}}{g_{\nu=0.2} V_m(\nu)}. \tag{32}$$

Dependences $V_m(\nu)$ were found using Equation (16). To find $g(\nu)$, the numerical solution of System (31) was first performed with random values of k_0, k_1, k_2 and k_3, and then the equilibrium constants were iteratively changed according to the Levenberg–Marquardt algorithm, until the best agreement between the experimental and calculated $\Delta E(\nu)$ dependences was achieved.

Figure 7 shows a comparison of the experimental and fitted $\Delta E(\nu)$ dependences at 983, 1023 and 1073 K. Table 1 gives the values of the equilibrium constants for Reactions (23)–(26), i.e., k_0, k_1, k_2 and k_3, at which the optimal coincidence of the curves was achieved.

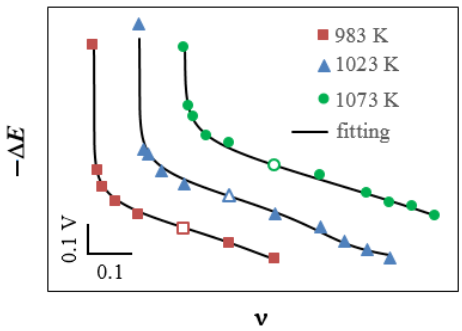

Figure 7. Experimental (symbols) and fitted (lines) dependences of the redox potential on the mole fraction of WO_3 in the Na_2WO_4–WO_3 melt. The curves have been shifted relative to each other to show them in one figure (the actual relative position of the experimental points is shown in Figure 3). The points that correspond to the standard melt $0.8Na_2WO_4$–$0.2WO_3$ ($\Delta E(\nu = 0.2) = 0$) are marked with blank symbols.

Table 1. Equilibrium constants of Reactions (23)–(26).

T, K	k_0, mol^{2}cm^{-6}	k_1	k_2	k_3
983	9.82×10^{-33}	8.40×10^{3}	3.05×10^{1}	1.77×10^{-13}
1023	1.09×10^{-28}	4.32×10^{2}	1.65	3.45×10^{-11}
1073	4.64×10^{-24}	1.44×10^{1}	5.82×10^{-2}	1.44×10^{-8}

Figure 8 shows the dependences of the concentrations of WO_2^{2+} WO_4^{2-}, $W_2O_7^{2-}$, $W_3O_{10}^{2-}$, $W_4O_{13}^{2-}$, and O^{2-} ions on the WO_3 mole fraction at 983, 1023 and 1073 K that correspond to the obtained values of the equilibrium constants. For some ν values, the concentrations of these ions and Na^+ ions are presented in Table 2. The calculation results indicate the following. The Na^+ and WO_4^{2-} ions predominate in molten sodium tungstate, which is consistent with the results of structural studies of this melt [29,31,32]. The fraction of other ions included in our model does not exceed 0.008%. The addition of even very small amounts of tungsten trioxide leads to a sharp decrease in the concentration of O^{2-} ions, which is especially noticeable at lower temperatures (Figure 8f). The WO_4^{2-} concentration, $[WO_4^{2-}]$, also decreases as the WO_3 mole fraction increases, and the decrease in $[WO_4^{2-}]$ is directly proportional to ν and almost does not depend on temperature up to ν ≈ 0.3 (Figure 8b).

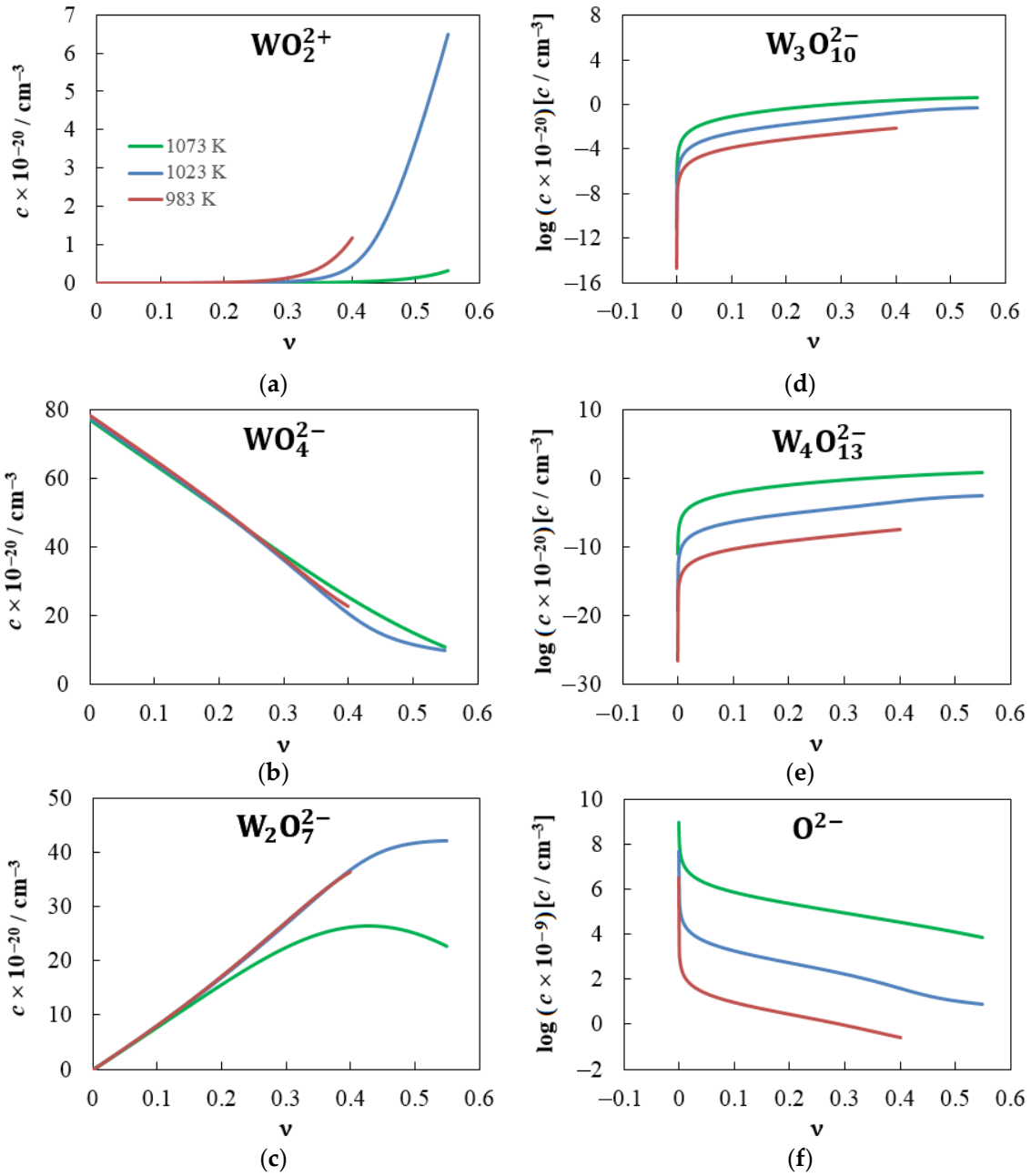

Figure 8. Dependences of the concentrations of tungsten-containing ions and O^{2-} ions on the mole fraction of tungsten trioxide in Na_2WO_4–WO_3 melts at 983, 1023 and 1073 K.

Table 2. Calculated values of ionic concentrations in Na_2WO_4–WO_3 melts.

WO_3 Mole Fraction (ν)	Concentrations of Ions (cm^{-3})						
	WO_2^{2+}	WO_4^{2-}	$W_2O_7^{2-}$	$W_3O_{10}^{2-}$	$W_4O_{13}^{2-}$	O^{2-}	Na^+
				983 K			
0	2.57×10^6	7.82×10^{21}	3.29×10^{15}	1.65×10^5	2.71×10^{-7}	3.29×10^{15}	1.56×10^{22}
0.1	2.72×10^{17}	6.52×10^{21}	8.15×10^{20}	1.21×10^{16}	5.90×10^9	9.25×10^9	1.47×10^{22}
0.2	2.42×10^{18}	5.17×10^{21}	1.72×10^{21}	6.77×10^{16}	8.77×10^{10}	2.76×10^9	1.38×10^{22}
0.3	1.64×10^{19}	3.70×10^{21}	2.70×10^{21}	2.35×10^{17}	6.71×10^{11}	8.96×10^8	1.28×10^{22}
0.4	1.22×10^{20}	2.30×10^{21}	3.62×10^{21}	6.79×10^{17}	4.17×10^{12}	2.59×10^8	1.16×10^{22}
				1023 K			
0	1.47×10^8	7.76×10^{21}	4.55×10^{16}	6.19×10^8	5.11	4.55×10^{16}	1.55×10^{22}
0.1	8.02×10^{16}	6.46×10^{21}	8.06×10^{20}	2.33×10^{17}	4.10×10^{13}	1.78×10^{12}	1.45×10^{22}
0.2	7.19×10^{17}	5.10×10^{21}	1.69×10^{21}	1.30×10^{18}	6.10×10^{14}	5.29×10^{11}	1.36×10^{22}
0.3	5.04×10^{18}	3.61×10^{21}	2.67×10^{21}	4.59×10^{18}	4.78×10^{15}	1.68×10^{11}	1.26×10^{22}
0.4	5.06×10^{19}	2.06×10^{21}	3.66×10^{21}	1.51×10^{19}	3.76×10^{16}	4.01×10^{10}	1.14×10^{22}
0.5	3.73×10^{20}	1.16×10^{21}	4.17×10^{21}	3.48×10^{19}	1.77×10^{17}	1.1×10^{10}	9.96×10^{21}
				1073 K			
0	1.52×10^{10}	7.68×10^{21}	9.21×10^{17}	7.68×10^{12}	1.10×10^9	9.21×10^{17}	1.54×10^{22}
0.1	1.90×10^{16}	6.37×10^{21}	7.80×10^{20}	6.62×10^{18}	9.65×10^{17}	7.51×10^{14}	1.43×10^{22}
0.2	1.53×10^{17}	5.07×10^{21}	1.57×10^{21}	3.36×10^{19}	1.24×10^{19}	2.36×10^{14}	1.34×10^{22}
0.3	7.77×10^{17}	3.76×10^{21}	2.25×10^{21}	9.38×10^{19}	6.72×10^{19}	9.02×10^{13}	1.23×10^{22}
0.4	3.46×10^{18}	2.53×10^{21}	2.63×10^{21}	1.90×10^{20}	2.35×10^{20}	3.51×10^{13}	1.12×10^{22}
0.5	1.51×10^{19}	1.50×10^{21}	2.52×10^{21}	2.92×10^{20}	5.84×10^{20}	1.30×10^{13}	9.77×10^{21}

The $W_2O_7^{2-}$ concentration initially increases in proportion to ν (Figure 8c), and the slopes are almost equal at lower temperatures. At 1073 K, the slope is noticeably lower and the maximum value is reached at ν = 0.43. Interestingly, the melt contains not only Na^+ cations and $W_2O_7^{2-}$ anions at ν = 0.5, contrary to the a priori assumption in [30,33–35]. Our calculations indicate that the fraction of $W_2O_7^{2-}$ in the $0.5Na_2WO_4$–$0.5WO_3$ melt (among other tungsten-containing ions) is only 72.7% at 1023 K and 51.2% at 1073 K.

The WO_2^{2+} concentration (Figure 8a) increases dramatically as ν increases. For example, at T = 983 K, the $[WO_2^{2+}] = 2.57 \times 10^6$ cm^{-3} at ν = 0, while the $[WO_2^{2+}] = 2.72 \times 10^{17}$ cm^{-3} at ν = 0.1. The WO_2^{2+} concentration, as is the case for the $W_2O_7^{2-}$ concentration, increases more slowly at 1023 K. At a high mole fraction of WO_3, the concentration of these cations is inferior to the concentrations of WO_4^{2-} and $W_2O_7^{2-}$ only by 1–2 orders of magnitude.

The concentrations of $W_3O_{10}^{2-}$ and $W_4O_{13}^{2-}$ ions increase as the WO_3 mole fraction and temperature increase (Figure 8d,e). The largest values of $d[W_3O_{10}^{2-}]/d\nu$ and $d[W_4O_{13}^{2-}]/d\nu$ are observed at low ν values. When T = 1073 K and $\nu \geq 0.4$, the $W_4O_{13}^{2-}$ concentration exceeds those of $W_3O_{10}^{2-}$ and WO_2^{2+} ions.

Thus, the proposed model allows us to calculate the equilibrium concentrations of ions, which are necessary for simulating electrodeposition from polytungstate melts and determining the composition of cathode products.

7. Conclusions

The problem of the ionic composition of Na_2WO_4–WO_3 melts was studied within the framework of a model that considers the equilibria between tungsten-containing and O^{2-} ions. The concentrations of O^{2-}, WO_2^{2+}, WO_4^{2-}, $W_2O_7^{2-}$, $W_3O_{10}^{2-}$, and $W_4O_{13}^{2-}$ ions were determined by fitting the EMF dependences calculated by Equation (32) to the experimental EMF values measured in the cell $Pt,\ O_2\,(air)|0.8Na_2WO_4 - 0.2WO_3 \,\vdots\, (1-\nu)Na_2WO_4 - \nu WO_3 \,|\, O_2(air), Pt$ with $0 \leq \nu \leq 0.55$ at 983, 1023 and 1073 K. Preliminarily, the adequacy of the approach was confirmed by measuring the EMF of the cell $Pt,\ O_2(air + Ar)|0.8Na_2WO_4 - 0.2WO_3 \,\vdots\, 0.8Na_2WO_4 - 0.2WO_3 \,|\, O_2(air), Pt$, and the stability of tungsten-containing anions and cations at experimental temperatures was established using DFT calculations.

The calculated dependences of the ion concentrations on the mole fraction of tungsten trioxide, taking into account the change in the density of the melt, indicate the following. In molten sodium

tungstate, Na^+ and WO_4^{2-} ions predominate, and the fraction of other ions is less than 0.01%. The addition of tungsten trioxide causes a sharp decrease in the concentration of O^{2-} ions and a sharp increase in the concentrations of WO_2^{2+}, $W_3O_{10}^{2-}$, and $W_4O_{13}^{2-}$. In addition, an increase in the WO_3 mole fraction leads to a decrease in the WO_4^{2-} concentration and an increase in the $W_2O_7^{2-}$ concentration. It was found that the $W_2O_7^{2-}$ ion does not dominate among other tungsten-containing ions, even in the $0.5Na_2WO_4$–$0.5WO_3$ melt, and its main competitors are WO_4^{2-} and WO_2^{2+} at 1023 K or WO_4^{2-}, $W_4O_{13}^{2-}$ and $W_3O_{10}^{2-}$ at 1073 K.

In conclusion, we emphasize that the main advantage of the proposed approach is the ability to obtain quantitative information about the change in the ionic composition of the melt that is associated with a change in temperature and/or the ratio of components in the initial oxide–salt mixture, based on a simple procedure for analyzing experimental data.

Author Contributions: Conceptualization, A.V.K.; methodology, A.V.K., A.S.V. and A.O.K.; software, A.V.K. and A.S.V.; validation, S.V.V. and O.V.G.; formal analysis, A.V.K., O.V.G. and O.L.S.; investigation, A.V.K., O.L.S., A.S.V. and A.O.K.; resources, Y.P.Z.; writing—original draft preparation, O.V.G. and A.V.K.; writing—review and editing, O.V.G. and A.V.K.; supervision, Y.P.Z. and S.V.V.; project administration, Y.P.Z. All authors have read and agreed to the published version of the manuscript.

Funding: This research received no external funding.

Data Availability Statement: Not applicable.

Acknowledgments: DFT calculations were performed on the hybrid cluster-type computer "URAN" at the N.N. Krasovskii Institute of Mathematics and Mechanics of the Ural Branch of the Russian Academy of Sciences.

Conflicts of Interest: The authors declare no conflict of interest.

References

1. Bartha, L.; Kiss, A.B.; Szalay, T. Chemistry of tungsten oxide bronzes. *Int. J. Refract. Met. Hard Mater.* **1995**, *13*, 77–91. [CrossRef]
2. El-Sayed, A.M.; Mousa, S.M.A. Some properties of sodium tungsten bronzes as a function of sodium concentration. *Ind. J. Chem. Technol.* **2005**, *12*, 304–308.
3. Sano, K.; Nitta, Y.; Ōno, Y. Transition temperature of superconductivity in sodium tungsten bronze—Theoretical study based on first-principles calculations. *J. Phys. Soc. Jpn.* **2020**, *89*, 113704. [CrossRef]
4. Lekshmi, I.C.; Hegde, M.S. Synthesis and electrical properties of cubic Na_xWO_3 thin films across the metal–insulator transition. *Mater. Res. Bull.* **2005**, *40*, 1443–1450. [CrossRef]
5. Raj, S.; Matsui, H.; Souma, S.; Sato, T.; Takahashi, T.; Chakraborty, A.; Sarma, D.D.; Mahadevan, P.; Oishi, S.; McCarroll, W.H.; et al. Electronic structure of sodium tungsten bronzes Na_xWO_3 by high-resolution angle-resolved photoemission spectroscopy. *Phys. Rev. B* **2007**, *75*, 155116. [CrossRef]
6. Bikberdina, N.Y.; Boronenko, M.P.; Gulyaev, P.Y.; Yunusov, R.D. Electrophysical properties of oxide bronze Na_xWO_3. *Bull. Yugorsk State Univ.* **2017**, *3*, 7–11. [CrossRef]
7. Petrov, L.A.; Shishmakov, A.B.; Vakarin, S.V.; Semerikova, O.L.; Melyaeva, A.A.; Mikushina, Y.V.; Zaykov, Y.P.; Chupakhin, O.N. Behavior of nanosized tungsten oxide bronzes produced by high-temperature electrolysis in model processes of desulfurization of petroleum products. *Russ. J. Inorgan. Chem.* **2014**, *59*, 7–10. [CrossRef]
8. Vakarin, S.V.; Melyaeva, A.A.; Semerikova, O.L.; Kondratuk, V.S.; Pankratov, A.A.; Plaksin, S.V.; Porotnikova, N.M.; Zaykov, Y.P.; Petrov, L.A.; Mikushina, Y.V.; et al. Catalase activity of coarse grained and nanosized oxide tungsten bronzes obtained by electrolysis of molten salts. *Russ. Chem. Bull.* **2011**, *60*, 1985–1988. [CrossRef]
9. Semerikova, O.L.; Vakarin, S.V.; Kosov, A.V.; Plaksin, S.V.; Pankratov, A.A.; Grishenkova, O.V.; Zaykov, Y.P.; Shishmakov, A.B.; Mikushina, Y.V.; Petrov, L.A. Electrochemical synthesis of nanohybrid systems based on copper and the oxide tungsten bronzes. *J. Electrochem. Soc.* **2019**, *166*, D792–D797. [CrossRef]
10. Wu, C.-M.; Naseem, S.; Chou, M.-H.; Wang, J.-H.; Jian, Y.-Q. Recent advances in tungsten-oxide-based materials and their applications. *Front. Mater.* **2019**, *6*, 49. [CrossRef]
11. Yi, L.; Zhao, W.; Huang, Y.; Wu, X.; Wang, J.; Zhang, G. Tungsten bronze $Cs_{0.33}WO_3$ nanorods modified by molybdenum for improved photocatalytic CO_2 reduction directly from air. *Sci. China Mater.* **2020**, *63*, 2206–2214. [CrossRef]
12. Wang, L.; Zhan, J.; Fan, W.; Cui, G.; Sun, H.; Zhuo, L.; Zhao, X.; Tang, B. Microcrystalline sodium tungsten bronze nanowire bundles as efficient visible light-responsive photocatalysts. *Chem. Commun.* **2010**, *46*, 8833–8835. [CrossRef]
13. Zimmer, A.; Gilliot, M.; Tresse, M.; Broch, L.; Tillous, K.E.; Boulanger, C.; Stein, N.; Horwat., D. Coloration mechanism of electrochromic Na_xWO_3 thin films. *Opt. Lett.* **2019**, *44*, 1104–1107. [CrossRef]
14. Tegg, L.; Cuskelly, D.; Keast, V.J. The sodium tungsten bronzes as plasmonic materials: Fabrication, calculation and characterization. *Mater. Res. Express* **2017**, *4*, 065703. [CrossRef]

15. Jie, S.; Guo, X.; Ouyang, Z. Tumor ablation using novel photothermal Na_xWO_3 nanoparticles against breast cancer osteolytic bone metastasis. *Int. J. Nanomed.* **2019**, *14*, 7353–7362. [CrossRef]
16. Azimirad, R.; Khademi, A.; Akhavan, J.; Moshfegh, A.Z. Growth of $Na_{0.3}WO_3$ nanorods for the field emission application. *J. Phys. D Appl. Phys.* **2009**, *42*, 205405. [CrossRef]
17. Wu, P.J.; Brahma, S.; Lu, H.H.; Huang, J.L. Synthesis of cesium tungsten bronze by a solution-based chemical route and the NIR shielding properties of cesium tungsten bronze thin films. *Appl. Phys. A* **2020**, *126*, 98. [CrossRef]
18. Kaliev, K.A.; Baraboshkin, A.N. Electrocrystallization of transition metal oxide bronzes from molten salts. In *Oxide Bronzes*; Spitsyn, V.I., Ed.; Nauka: Moscow, Russia, 1982; pp. 137–175.
19. Vakarin, S.V. *Oriented Growth of Tungsten Bronzes at the Melts Electrolysis*; UB RAS: Ekaterinburg, Russia, 2005. (In Russian)
20. Kosov, A.V.; Semerikova, O.L.; Vakarin, S.V.; Grishenkova, O.V.; Trofimov, A.A.; Leonova, A.M.; Leonova, N.M.; Zaikov, Y.P. Photovoltaic response of silicon wafers treated in the K_2WO_4-Na_2WO_4-WO_3 melt. *J. Electrochem. Soc.* **2021**, *168*, 126503. [CrossRef]
21. Kosov, A.V.; Semerikova, O.L.; Vakarin, S.V.; Zaykov, Y.P. Electrochemical behavior of the nickel/oxide tungsten bronze system at cyclic potential sweep. *Russ. Metall.* **2019**, *2019*, 803–808. [CrossRef]
22. Kosov, A.V.; Semerikova, O.L.; Vakarin, S.V.; Pankratov, A.A.; Plaksin, S.V.; Korzun, I.V.; Akashev, L.A.; Zaykov, Y.P. Electrochemical synthesis of tetragonal oxide tungsten bronze nanofilms on platinum. *Russ. Metall.* **2017**, *2017*, 152–157. [CrossRef]
23. Kosov, A.V.; Semerikova, O.L.; Vakarin, S.V.; Pankratov, A.A.; Plaksin, S.V.; Zaykov, Y.P. Formation of nanocrystalline tetragonal oxide tungsten bronzes on platinum. *Russ. Metall.* **2017**, *2017*, 158–162. [CrossRef]
24. Vakarin, S.V.; Semerikova, O.L.; Kosov, A.B.; Pankratov, A.A.; Plaksin, S.V.; Korzun, I.V.; Akashev, L.A.; Zaikov, Y.P. Electrochemical deposition of nanocrystalline tungsten bronze films on platinum. *Int. J. Adv. Res.* **2015**, *3*, 691–700.
25. Shurdumov, B.K. On the mechanism of the formation of oxide tungsten bronzes of alkali metals during the electrolysis of high-viscosity melts of tungstate phosphate systems. *Izvestiya Vuzov Khimiya Khimicheskaya Tekhnologiya* **2001**, *44*, 152–155. (In Russian)
26. Khubolov, B.M. Electrocrystallization of thin films of sodium—Tungsten bronzes. In *Physical and Chemical Aspects of the Study of Clusters, Nanostructures and Nanomaterials*; Tver State University: Tver, Russia, 2020; pp. 213–221.
27. Khubolov, B.M. Electrochemical synthesis of oxide tungsten bronze powders. In *Physical and Chemical Aspects of the Study of Clusters, Nanostructures and Nanomaterials*; Tver State University: Tver, Russia, 2020; pp. 738–745.
28. Drobasheva, T.I.; Snezhkov, V.I. Electrocrystallization and properties of alkali-metal tungsten and molybdenum bronzes. *Inorg. Mater.* **1998**, *34*, 1162–1165.
29. Okada, K.; Miyake, M.; Iwai, S.; Ohno, H.; Furukawa, K. Structural analysis of molten Na_2WO_4. *J. Chem. Soc. Faraday Trans. 2* **1978**, *74*, 1141–1148. [CrossRef]
30. Miyake, M.; Okada, K.; Iwai, S.; Ohno, H.; Furukawa, K. Structural analysis of molten $Na_2W_2O_7$. *J. Chem. Soc. Faraday Trans. 2* **1978**, *74*, 1880–1884. [CrossRef]
31. Voron'ko, Y.K.; Sobol', A.A. Influence of cations on the vibrational spectra and structure of $[WO_4]$ complexes in molten tungstates. *Inorg. Mater.* **2005**, *41*, 420–428. [CrossRef]
32. Voronko, Y.K.; Sobol, A.A.; Shukshin, V.E. Raman scattering study of molten alkali-metal molybdates and tungstates rich in basic oxides. *Inorg. Mater.* **2014**, *50*, 837–843. [CrossRef]
33. Wang, J.; You, J.; Wang, M.; Lu, L.; Wan, S.; Sobol, A.A. In-situ studies on the micro-structure evolution of $A_2W_2O_7$ (A = Li, Na, K) during melting by high temperature Raman spectroscopy and density functional theory. *Spectrochim. Acta A* **2017**, *185*, 188–196. [CrossRef]
34. Wang, J.; You, J.L.; Sobol, A.A.; Lu, L.M.; Wang, M.; Wu, J.; Lv, X.M.; Wan, S.M. In-situ high temperature Raman spectroscopic study on the structural evolution of $Na_2W_2O_7$ from the crystalline to molten states. *J. Raman Spectrosc.* **2017**, *48*, 298–304. [CrossRef]
35. Wang, J.; You, J.L.; Wang, Y.Y.; Wang, M.; Jun, W.U. In-situ Raman spectroscopic study of the molten tungstates in Li_2O-WO_3 binary system. *Chin. J. Light Scatt.* **2016**, *28*, 149–152.
36. Gunzi, K.; Kohsaka, S.; Yokokawa, T.E.m.f. measurements of molten oxide mixtures IV. Sodium oxide + molybdenum trioxide. *J. Chem. Thermodyn.* **1979**, *11*, 553–557. [CrossRef]
37. Khvatov, A.Y.; Baraboshkin, A.N.; Tarasova, K.P. Study of the ionic composition of a tungstate melt by the EMF method. *Elektrokhimiya* **1985**, *21*, 1657–1660. (In Russian)
38. Afonichkin, V.K.; Leontiev, V.N.; Komarov, V.E. Equilibrium electrode potentials of tungsten in melts of the Na_2WO_4–WO_3 system. *Elektrokhimiya* **1993**, *29*, 341–347. (In Russian)
39. Smirnov, M.; Stepanov, V. Density and surface tension of molten alkali halides and their binary mixtures. *Electrochim. Acta* **1982**, *27*, 1551–1563. [CrossRef]
40. Khudorozhkova, A.O.; Isakov, A.V.; Kataev, A.A.; Red'kin, A.A.; Zaikov, Y.P. Density of KF–KCl–KI melts. *Russ. Metall.* **2020**, *2020*, 918–924. [CrossRef]
41. Soler, J.M.; Artacho, E.; Gale, J.D.; Garcia, A.; Junquera, J.; Ordejon, P.; Sanchez-Portal, D. The SIESTA method for ab initio order-N materials simulation. *J. Phys. Condens. Matter* **2002**, *14*, 2745–2779. [CrossRef]
42. Perdew, J.P.; Burke, K.; Ernzerhof, M. Generalized gradient approximation made simple. *Phys. Rev. Lett.* **1996**, *77*, 3865–3868. [CrossRef]

43. Nose, S. A unified formulation of the constant temperature molecular dynamics methods. *J. Chem. Phys.* **1984**, *81*, 511–519. [CrossRef]
44. Bychin, V.P.; Antonov, A.A. Some physical and chemical properties of the Na_2WO_4–WO_3. In Chemistry and Technology of Molybdenum and Tungsten. In Proceedings of the III All-Union Meeting, North Caucasus Mining and Metallurgical Institute, Ordzhonikidze, USSR, 7 October 1977; pp. 63–64. (In Russian).